



HAL
open science

Regulation of pendrin by pH: dependence on glycosylation

Anie Azroyan, Kamel Laghmani, Gilles Crambert, David Mordasini, Alain Doucet, Aurélie Edwards

► **To cite this version:**

Anie Azroyan, Kamel Laghmani, Gilles Crambert, David Mordasini, Alain Doucet, et al.. Regulation of pendrin by pH: dependence on glycosylation. *Biochemical Journal*, 2011, 434 (1), pp.61-72. 10.1042/BJ20101411 . hal-00560691

HAL Id: hal-00560691

<https://hal.science/hal-00560691>

Submitted on 29 Jan 2011

HAL is a multi-disciplinary open access archive for the deposit and dissemination of scientific research documents, whether they are published or not. The documents may come from teaching and research institutions in France or abroad, or from public or private research centers.

L'archive ouverte pluridisciplinaire **HAL**, est destinée au dépôt et à la diffusion de documents scientifiques de niveau recherche, publiés ou non, émanant des établissements d'enseignement et de recherche français ou étrangers, des laboratoires publics ou privés.

REGULATION OF PENDRIN BY pH: DEPENDENCE ON GLYCOSYLATION

Running title: Mathematical Modeling of Pendrin Activity

**Anie Azroyan^{*,†}, Kamel Laghmani^{*,†}, Gilles Crambert^{*,†}, David Mordasini^{*,†},
Alain Doucet^{*,†}, and Aurélie Edwards^{*,†,‡}**

From UPMC Univ Paris 06, Univ Paris 05, and INSERM, UMRS872^{*}, and CNRS ERL7226[†],
Laboratoire de génomique, physiologie et physiopathologie rénales,
Centre de Recherche des Cordeliers, 75006, Paris, France;

[‡]Department of Chemical and Biological Engineering, Tufts University, Medford, MA, USA.

Corresponding author:

Aurélie Edwards

Centre de Recherche des Cordeliers Equipe 3, 15 rue de l'Ecole de Médecine, 75270 Paris
Cedex 6, France.

Tel: (33) 1 44 41 37 18.

Fax: (33) 1 44 41 37 17.

E-mail: aurelie.edwards@upmc.fr

SYNOPSIS

Mutations of the anion exchanger pendrin are responsible for Pendred syndrome, an autosomal recessive disease characterized by deafness and goiter. Pendrin is highly expressed in kidney collecting ducts, where it acts as a chloride/bicarbonate exchanger and thereby contributes to the regulation of acid-base homeostasis and blood pressure. This study aimed to characterize the intrinsic properties of pendrin. Mouse pendrin was transfected in HEK293 and OKP cells; its activity was determined by monitoring changes in intracellular pH induced by variations of trans-membrane anion gradients. Combining measurements of pendrin activity with mathematical modeling, we found that its affinities for Cl^- , HCO_3^- and OH^- vary with intracellular pH, resulting in increased activity at low intracellular pH. Pendrin maximal activity was also stimulated at low extracellular pH, suggesting the presence of intra- and extracellular proton regulatory sites. We identified 5 putative pendrin glycosylation sites, only two of which are used. Mutagenesis-induced disruption of pendrin glycosylation did not alter its cell surface expression, polarized targeting to the apical membrane and basal activity, but fully abrogated its sensitivity to extracellular pH. The hereto unknown regulation of pendrin by external pH may constitute a key mechanism in controlling ionic exchanges across the collecting duct and inner ear.

Word count: 200

Keywords: pendrin; anion exchanger; mathematical modeling; transport kinetics; glycosylation; pH.

Abbreviations: B-IC, type-B intercalated cells; CCD, cortical collecting duct; DIDS, 4,4'-diisothiocyanatostilbene-2,2'-disulfonate.

INTRODUCTION

Pendred syndrome is an autosomal recessive disease characterized by deafness and goiter [1]. It is associated with mutations of the *PDS* gene which encodes pendrin, an anion exchanger that is a member of SLC26 family (Slc26a4). Pendrin exchanges extracellular chloride against either intracellular bicarbonate or iodide or formate [2-4]. The Cl^-/I^- and $\text{Cl}^-/\text{HCO}_3^-$ exchange functions of pendrin account for its role in iodide organification in the thyroid and in pH homeostasis of endolymph respectively, which are altered in Pendred syndrome [5, 6]. Even though patients with Pendred syndrome display no clinical signs beyond the thyroid and inner ear, pendrin is expressed in many tissues including mammary glands [7], uterus [8], testis [9], placenta [9], and kidneys [10]. Kidneys even display a higher expression level of pendrin mRNAs than the thyroid gland and inner ear.

In the kidney, pendrin is expressed at the apical border of the type-B intercalated cells (B-IC) present in the cortical collecting duct (CCD). B-ICs play a major role in the regulation of acid-base balance by mediating bicarbonate secretion through an apical $\text{Cl}^-/\text{HCO}_3^-$ exchanger functioning in series with a basolateral plasma membrane H^+ -ATPase. Recent studies have shown that HCO_3^- secretion in CCDs is abolished in pendrin knockout mice, which indicates that apical $\text{Cl}^-/\text{HCO}_3^-$ exchange in B-ICs is fully mediated by pendrin [10, 11]. Accordingly, both the expression and the activity of the apical anion exchanger are upregulated in CCD after induction of metabolic alkalosis by either administration of aldosterone or NaHCO_3 loading, and aldosterone-induced metabolic alkalosis is more severe in pendrin knockout mice than in controls [12].

In addition, B-ICs are sites of chloride reabsorption through the apical $\text{Cl}^-/\text{HCO}_3^-$ exchanger in series with basolateral chloride channels *ClCK*. Chloride reabsorption in CCDs is fully abolished in pendrin knockout mice [11], indicating that pendrin-mediated transcellular transport in B-ICs is the only pathway for chloride reabsorption in CCDs. Moreover, the expression of pendrin in the kidney of rats fed different amounts of chloride is inversely correlated with the urinary excretion of chloride, independently of the accompanying cation and acid-base status [13, 14]. This suggests a major role for pendrin in the regulation of chloride balance.

Finally, it was reported recently that coupling of pendrin with the Na^+ -driven $\text{Cl}^-/\text{HCO}_3^-$ exchanger (NDCBE/Slc4a8) mediates electroneutral reabsorption of NaCl in the CCD [15]. The presence of this thiazide-sensitive pathway for NaCl reabsorption, which operates in parallel with the amiloride-sensitive epithelial sodium channel, likely accounts for the fact that isolated alteration of Cl^- transport in the distal nephron can impact blood pressure [16-19] and that pendrin knockout mice are protected against mineralocorticoid/salt-induced hypertension [12].

The importance of pendrin in mediating Na^+ and Cl^- reabsorption and HCO_3^- secretion in the CCD, and in regulating acid-base balance, extracellular volume and blood pressure, underlies the need to characterize its intrinsic properties, which have remained poorly documented until now. The purpose of this study was to functionally characterize pendrin using in vitro expression models. Our major findings are that pendrin activity is modulated by pH and that this regulation depends on pendrin glycosylation.

EXPERIMENTAL

Cloning of mouse pendrin cDNA. Mouse cDNA was generated from total RNA using Superscript III RT (Invitrogen). The coding sequence of pendrin was amplified by PCR using the platinum *pfx* polymerase (Invitrogen) and the following primers: sense, 5'GTCATCCC-TCGTCGCATC3' and reverse 5'TCTCAGGAAGCAAGTCTACGC3'. After a subsequent A-tailing with Taq polymerase, the mouse pendrin coding sequence was subcloned into a pTarget mammalian expression vector following the manufacturer's protocol (Promega, Madison WI).

Site-directed mutagenesis. Asparagines at positions 167, 172, 241, 475 and 567, predicted by the NetNGlyc 1.0 Server to be putative N-glycosylation sites, were mutated to alanines using site-directed mutagenesis on the wild-type pendrin-pTarget construct. Site-specific mutagenesis was performed using the QuickChange™ site-directed mutagenesis kit (Stratagene, La Jolla, USA), and mutations were confirmed by sequencing the plasmid DNA (GATC Biotech AG, Deutschland). All mutants were then transiently transfected into Human Embryonic Kidney 293 (HEK293) cells for protein expression assays and stably transfected in Opossum Kidney (OKP) cells for transport activity assays.

Cell culture and transfection. OKP and HEK293 cells were cultured in Dulbecco's modified Eagle's medium (Gibco, Invitrogen) supplemented with 2mM glutamine and 10% fetal bovine serum (Gibco Invitrogen), penicillin (100 U/ml), and streptomycin (100 µg/ml) at 37°C in a 5% CO₂/95% O₂ mix. Cells grown in 60 mm dishes were transfected with 1µg of pendrin cDNA construct using Lipofectamine Plus kit (Invitrogen) according to the manufacturer's protocol. Transiently transfected cells were studied 48 h after transfection for protein expression and activity. For stable transfections, cells were selected by their resistance to G418 (500 µg/ml) (Invitrogen). Single clones were isolated and placed into the separate wells of a 24 well plate. Cells were grown to confluence sufficient for detection of pendrin by western blotting and immunostaining. For experiments, one clone was extensively analysed. Non-transfected cells were used as control.

Cell surface biotinylation. Cells were placed on ice and rinsed twice with a cold rinsing solution at pH 8 containing PBS, 1 mM MgCl₂, and 0.1 mM CaCl₂ (PBS-Ca-Mg). Cells were then incubated at 4°C for 1 h in PBS-Ca-Mg pH8, containing 1 mg/ml NHS-biotin. Biotinylation was stopped by washing 3 times with ice-cold PBS-Ca-Mg supplemented with 100 mM glycine. Cells were then washed 3 times in PBS-Ca-Mg. Washed cells were lysed for 20 min at 4 °C in lysis buffer (150 mM NaCl, 5 mM EDTA, 50 mM Tris/Hepes, pH 7.5; 1% (v/v) Triton X-100) containing protease inhibitors (Complete 1697498, Roche Diagnostics). To quantify protein amounts, 10µg of total cell extract from each sample was used to provide a measure of total pendrin expression, and 50µg of cell lysates were incubated with avidin beads (Sigma) overnight at 4°C. After overnight incubation, samples were centrifuged at 16,000 rpm for 5 min, and the supernatant (the intracellular fraction) was removed. Avidin beads were then washed 3 times with lysis buffer, twice with high salt buffer (500mM NaCl, 5mM EDTA, 50mM Tris, 0.1% triton X100, pH7.5) and once with no salt buffer (10mM Tris pH 7.5) and then denaturated for 20 minutes at 65°C with Laemmli denaturing buffer and subjected to SDS-PAGE and immunoblotting.

Immunoblotting. Western blotting was performed on whole cell lysates. HEK293 or OKP cells were solubilised in high-salt lysis buffer (HSB) containing 500 mM NaCl, 50 mM Tris (pH 8), 1% Triton X100, 0.1% SDS, with the complete protease inhibitor cocktail (Roche Diagnostics). For enzymatic deglycosylation 20 µg of proteins were treated with either N glycosidase F or endoglycosidase H following the manufacturer's protocols. Proteins were resolved for 3 h at 300 V in 10% SDS-PAGE (Bio-Rad) and transferred to nitrocellulose membrane (GE Healthcare) for 2 hours at 600 mA. Blots were blocked using 5% non-fat milk in TBS

0.1% Tween 20 for 1 h and then incubated overnight with primary anti-pendrin antibody diluted 1:5000 in TBS 0.1% Tween 20. Blots were then washed 3 times with TBS 0.1% Tween 20, and incubated with horseradish peroxidase-conjugated goat anti rabbit IgG (Promega, Madison, WI, USA) 1:10000 in TBS 0.1% Tween 20. Blots were washed as described above and assayed with ECL using SuperSignal Substrate (Pierce, Rockford, IL, USA) and captured on a light sensitive imaging film (Kodak).

The anti-pendrin antibody (gift from Dr D Eladari), a rabbit polyclonal antibody directed against a peptide corresponding to the C-terminal domain of mouse pendrin (amino acids 630 to 643), has been characterized previously [20, 21].

Immunofluorescence. OKP cells plated at confluent density on 12 mm transwell porous cell culture inserts (0.4 μm pore, Costar) for 7 days and HEK293 cells grown on glass coverslips were washed twice with an ice-cold PBS solution at pH 8 containing 1 mM MgCl_2 and 0.1 mM CaCl_2 , and were then placed at 4°C for 1h in PBS solution containing 1 mg/ml EZ-Link Sulfo-NHS-LC-LC-Biotin (Pierce). After 3 washes with PBS, cells were fixed with 4% paraformaldehyde (Electron Microscopy Sciences, Hatfield, PA) for 30 min at room temperature, then washed 3 times with PBS and permeabilized with 0.1% Triton X100 for 15 min. Cells were blocked for 30 min with 3% normal goat serum (Vector Laboratories) and incubated with anti-pendrin antibody diluted 1:400 in 3% normal goat serum for 1h. After 3 washes with PBS, cells were incubated for 1h in the dark with FITC-conjugated goat anti-rabbit IgG diluted 1:100 and Cy5-conjugated streptavidin (Sigma Aldrich) at 1:100. Filters were excised from the filter cup with a razor blade and mounted with Vectashield H1200 (Vector Laboratories) mounting media containing 4,6-diamidino 2-phenylindole dihydrochloride for nuclei staining. Slides were visualised with a Zeiss LSM 510 laser-scanning microscope using appropriate filters (Carl Zeiss, Germany).

Intracellular pH measurement. Activity of pendrin in transfected cells was assessed based on the rate of variation of intracellular pH (pH_i) in response to the generation of transmembrane gradients of Cl^- , HCO_3^- or OH^- concentration. The activity of pendrin was calculated as the difference between the rate of pH variation in transfected cells and that in non-transfected cells in the same experimental series. Changes in transmembrane ion gradients were obtained by varying the composition of the extracellular medium, as indicated in the *Results* section. For pH_i measurements, HEK293 cells grown to confluence on glass coverslips coated with 0.5 mg/ml poly D-lysine (Sigma) were incubated for 30 min at 37°C in the presence of 5 μM pH sensitive dye 2',7'-bis(2-carboxyl)-5(6)-carboxy-fluorescein (BCECF) (Invitrogen) in isotonic solutions. Changes in intracellular pH were monitored at excitation wavelengths of 500 and 450 nm, at 37°C, in a FluoroMax3 spectrofluorometer (Jobin Yvon, Horiba). Three-point calibration curves (pH 6.0, 7.0 and 8.0) were established using KCl/nigericine. Cl^- -containing solutions consisted of NaCl at concentrations varying from 0.5 mM to 120 mM, Na-gluconate, KCl, and K-gluconate. All solutions contained 0.2 mM KH_2PO_4 , 0.8 mM K_2HPO_4 , 1 mM Ca-gluconate, 1 mM Mg-gluconate and 10 mM HEPES. For Cl^- -free solutions, all Cl^- containing salts were replaced with gluconate salts. For HCO_3^- -containing solutions Na-gluconate was replaced isosmotically with NaHCO_3 . Bicarbonate containing solutions were prepared temporarily to intracellular pH measurements. The actual concentration of bicarbonate was calculated as explained in **Appendix A**.

The intrinsic buffering power (β_i ; mM H^+ /pH unit) was measured in transfected and non-transfected HEK293 cells using the NH_4^+ pulse method. To eliminate all pendrin activity the measurements were done in the presence of 0.5 mM DIDS. Cells were initially loaded with BCECF in Na^+ - and bicarbonate-free isotonic solutions. NaCl was iso-osmolarly replaced with NMDGCl. The ΔpH_i of cell alkalinisation was measured after the addition of 20 mM NH_4Cl by iso-osmolar replacement of NMDGCl. The base equivalent transport flux was cal-

culated by multiplying the buffering power ($\text{mM H}^+/\text{pH unit}$) by the transport rate (pH unit/min) and expressed in mM/min .

When tested, pharmacological agents (Sigma Aldrich) were added simultaneously with BCECF. They were dissolved in DMSO (Sigma, 1% final concentration), and the same concentration of DMSO was added to controls.

Measurement of intracellular chloride concentration. Pendrin-transfected HEK293 cells grown to confluence on glass coverslips were labelled for 24 hours with 5 mM SPQ (6-methoxy-N-(3-sulfopropyl)-quinolinium, inner salt) (Molecular Probes) in sterile DMEM medium supplemented with 10% bovine serum. Afterwards, cells were washed extensively in isotonic buffer at pH 7.4, prior to 30 min incubation in the same buffer at 37°C . The isotonic buffers were either Cl^- -free solutions or Cl^- -containing solutions consisting of NaCl at concentrations varying between 4 mM and 120 mM . After incubation cells were washed again 5 times and SPQ fluorescence was measured in a FluoroMax3 spectrofluorometer at excitation and emission wavelengths of 365 nm and 443 nm respectively. Calibration curves were established using KCl/nigericine (5 μM)/tributyltine (10 μM). For calibration Cl^- -containing solutions consisted of KCl at concentrations varying from 4 mM to 120 mM , Na-gluconate, Mg-gluconate, Ca-gluconate, K-gluconate and Hepes.

Statistics. Values are expressed as means \pm S.E. The significance of differences between mean values was evaluated using paired or unpaired t test or analysis of variance as appropriate. $p < 0.05$ was considered statistically significant.

RESULTS

Expression of pendrin protein in HEK293 cells. We first determined the expression of pendrin protein and its location in HEK293 cells stably transfected with mouse pendrin cDNA. **Figure 1** shows that all the cells derived from a single clone displayed pendrin-positive staining. Pendrin immunoreactivity was mainly present at the plasma membrane since it colocalized with biotin. In contrast, non-transfected or mock-transfected cells did not show any positive stain for pendrin (data not shown).

Measurements of pendrin activity. We next characterized the functional expression of pendrin by determining the rate of ion transport in either Cl^-/OH^- or $\text{Cl}^-/\text{HCO}_3^-$ exchange mode in pendrin cDNA-transfected cells. Previous studies demonstrated that pendrin functions in Cl^-/OH^- , $\text{Cl}^-/\text{HCO}_3^-$, or $\text{Cl}^-/\text{formate}$ electroneutral exchange mode [22, 23].

Cl^-/OH^- exchange. Cells were first incubated in a Cl^- -free medium for 30 min at 37°C and then monitored for changes in intracellular pH (pH_i) after addition of extracellular Cl^- . **Figure 2A** shows that the addition of extracellular Cl^- (120 mM) caused a more rapid cellular acidification in pendrin-transfected cells than in non-transfected cells. This phenomenon was reversed after the cells were switched back to a Cl^- -free medium (**Figure 2B**). The initial rate of cell acidification, corresponding to the forward rate of Cl^-/OH^- exchange, was ~ 0.3 and ~ 0.04 $\text{pH unit}\cdot\text{min}^{-1}$ in transfected and non-transfected cells respectively. The backward rate of Cl^-/OH^- exchange was ~ 0.2 in transfected cells and ~ 0.03 $\text{pH unit}\cdot\text{min}^{-1}$ in non-transfected cells.

$\text{Cl}^-/\text{HCO}_3^-$ exchange. In these series of experiments, cells were first incubated in a bicarbonate-free and Cl^- -containing medium for 30 min at 37°C, and then monitored for pH_i changes after switching to a bicarbonate-containing and Cl^- -free medium. As shown in **Figure 2C**, the concomitant addition of bicarbonate (25 mM) and removal of chloride from the medium caused a transient acidification of both pendrin-transfected and non-transfected cells that is likely accounted for by CO_2 entry. Afterwards, a more rapid intracellular alkalinisation was observed in pendrin-transfected cells than in non-transfected cells. The initial rate of cell alkalinisation, corresponding to the rate of $\text{Cl}^-/\text{HCO}_3^-$ exchange, was ~ 0.8 and ~ 0.2 $\text{pH unit}\cdot\text{min}^{-1}$ in transfected and non-transfected cells respectively.

We also confirmed that pendrin is inhibited by 4,4'-diisothiocyanatostilbene-2,2'-disulfonate (DIDS), as previously described [22]. Pendrin activity determined under forward $\text{Cl}^-/\text{HCO}_3^-$ exchange mode was fully inhibited by 0.5 mM DIDS: (in $\text{mM}\cdot\text{min}^{-1} \pm \text{SE}$) Control, 20.1 ± 1.0 ; DIDS, 1.4 ± 1.4 ; $n = 6$, $p < 0.001$.

Effect of pH on pendrin activity. We examined whether pendrin is regulated by pH by measuring its activity while either the extracellular (pH_e) or the intracellular (pH_i) pH was varied. In the first series of experiments, the cells were incubated in a Cl^- -free medium at $\text{pH}_e = 7.4$; their pH_i rose to an equilibrium value of 7.85. At $t = 0$, the cells were suddenly exposed to a 120 mM Cl^- medium of variable pH_e . The bath switch resulted in Cl^- influx and OH^- efflux. As shown in **Figure 3A**, the initial flux of OH^- out of the cell was found to increase with decreasing pH_e .

To examine the effect of intracellular pH on the activity of the exchanger, the cells were incubated in a 120 mM Cl^- medium at variable pH_e (6.0, 7.4, and 8.0); their equilibrium pH_i then reached varying values (6.2, 7.0, and 7.5). At $t = 0$, the cells were exposed to a Cl^- -free medium at a fixed pH_e of 8.0, resulting in Cl^- efflux and OH^- influx into the cells. The initial rate of cell alkalinization was seen to increase with decreasing pH_i , as displayed in **Figure 3B**.

A decrease in extracellular or intracellular pH enhances the gradient for OH^- efflux or influx, respectively, and therefore might account for the observed increase in pendrin activity.

To evaluate whether the pH dependence reflects a true regulation of pendrin or a concentration gradient effect, we then sought to determine the kinetics parameters of pendrin.

Kinetic parameters of pendrin. To calculate the affinities of pendrin to Cl^- , OH^- and HCO_3^- , we first determined pendrin activity by measuring pH_i variations in the presence of different anion concentrations, in several exchange modes. In all experiments, the activity of pendrin was calculated as the difference in the initial rate of pH_i variation between pendrin-transfected and non-transfected cells. Next, the affinities were calculated based on a theoretical model of pendrin-mediated ion transport.

Activity of pendrin as a function of external chloride. Cells were pre-incubated in a Cl^- -free medium, then switched to a medium containing different concentrations of Cl^- (0.5 to 100 mM), and the initial rate of acidification was measured. As expected, increasing extracellular Cl^- concentration increased pendrin activity in a saturable fashion. Linearizing the data according to the Lineweaver-Burk equation yielded an apparent external Cl^- affinity of 1.35 mM and a V_{\max} of 0.3 pH unit. min^{-1} (**Figure 4A**).

Activity of pendrin as a function of internal chloride. To determine the apparent intracellular affinity of pendrin for Cl^- , we measured the initial rate of alkalisation during backward Cl^-/OH^- exchange. Thus, after pre-incubation in Cl^- -free medium, the cells were switched to a medium containing various concentrations of Cl^- and the change in pH_i was monitored. When pH_i equilibrium was achieved, the cells were switched back to a Cl^- -free medium and the initial rate of alkalisation was determined. The internal concentration of Cl^- at the onset of the alkalisation phase was determined by SPQ fluorescence in separate experiments. Using this protocol we were able to vary the intracellular concentration of Cl^- from 0.5 to 50 mM. This was accompanied by a saturable activation of pendrin, and an apparent internal Cl^- affinity of 24 mM and a V_{\max} of 0.2 pH unit. min^{-1} were derived from the Lineweaver-Burk plot (**Figure 4B**).

Activity of pendrin as a function of external bicarbonate. Following pre-incubation in a bicarbonate-free and Cl^- -containing medium, the cells were switched to a Cl^- -free medium containing various concentrations of HCO_3^- and the initial rate of alkalisation was measured. Bicarbonate was added at concentrations ranging from 1 to 25 mM, and the corresponding actual concentrations of HCO_3^- in the medium were calculated as described in **Appendix A**. A Lineweaver-Burk plot of the data gave an apparent external HCO_3^- affinity of 2.6 mM and a V_{\max} of 0.8 pH unit. min^{-1} (**Figure 4C**).

The curves representing the initial flux across pendrin as a function of external or internal anion concentrations (**Figure 4A-C**) were then used to determine the kinetic parameters of the exchanger. We examined different models (such as the bi bi cyclic reaction scheme, the six-state ping-pong model, an eight-state exchanger scheme) and obtained the best fit to the data using the ping-pong mechanism depicted in **Figure 5**. According to this scheme, after Cl^- binds to the empty carrier on one side, it is translocated to the other side; only after it is released can the other ion (HCO_3^- or OH^-) bind to the carrier and be translocated back in the opposite direction. Note that this kinetic scheme is identical to that assumed for the $\text{Cl}^-/\text{HCO}_3^-$ exchanger AE1 [24]. To fully characterize dynamic transport across pendrin, 4 kinetic parameters per ionic species must be determined: the external and internal binding affinities, and the forward and backward translocation rates.

The flux equations are given in **Appendix B**. As discussed therein, the experimental curves in this study can only yield 6 independent parameters, out of a total of 10 (6 affinities and 4 independent translocation rates). We therefore assumed that the internal and external binding affinities of each ion are equal, and we fixed the forward (external) Cl^- translocation rate (denoted P_{Cl}^e). The remaining 6 independent parameters (the affinities to Cl^- , HCO_3^- , and

OH^- ; the forward rates for HCO_3^- and OH^- ; and the backward rate for Cl^-) were then fitted to the experimental data.

Analysis of the experimental results revealed that it was not possible to fit the data shown in **Figures 4A and 4B** simultaneously without accounting for the modulating effect of internal pH (~ 8.0 in the Cl^- influx experiments, vs. ~ 7.0 in the Cl^- efflux experiments) on pendrin activity. Moreover, assuming that the kinetic parameters of pendrin are independent of pH_i , the model predicts that the driving force in the experiment displayed in **Figure 3B** remains constant, that is, the flux should remain approximately the same as pH_i varies between 6.2 and 7.5. Thus, these two sets of results strongly suggest that pH_i variations intrinsically modify the kinetics of the transporter, independently of transmembrane concentration gradients. We accounted for this effect by assuming that the binding affinities of Cl^- and OH^- vary with internal pH.

Fitted parameter values are given in **Table 1**. As described in **Appendix B**, the fitted values of the affinities, and of the translocation rates relative to $\text{P}_{\text{Cl}^-}^c$, depend very little on the value of $\text{P}_{\text{Cl}^-}^c$. The affinity of pendrin for Cl^- and OH^- was respectively calculated as 3 mM and 1.4×10^{-6} M at $\text{pH}_i = 8.0$, and as 75 mM and 2.6×10^{-7} M at $\text{pH}_i = 7.0$. Predicted flux values based upon these parameters are in good agreement with measured values, as displayed in **Figure 4**.

We then sought to interpret the effect of external pH depicted on **Figure 3A**. If pH_e had no intrinsic effect on the kinetic parameters of pendrin, the mathematical model would predict a constant flux in these experiments. Indeed, the ‘effective’ concentration of Cl^- (i.e., its concentration divided by its affinity) in the bath was much greater than that of OH^- both in the bath and within the cell, so that the intracellular concentration of OH^- was the rate-limiting factor that determines the magnitude of the flux. Given that the initial pH_i was constant in these experiments, the flux at $t = 0$ should have remained constant in the absence of an intrinsic effect of pH_e . The fact that the flux decreased with increasing pH_e strongly suggests that lowering pH_e stimulates pendrin activity.

Glycosylation of pendrin. Immunodetection of mouse pendrin transiently expressed in HEK293 cells reveals two bands at ~ 130 kDa and ~ 90 kDa (**Figure 6A**). Treatment with endoglycosidase H, which hydrolyzes only the high mannose sugars, did not alter the 130 kDa band and slightly reduced to ~ 85 kDa the apparent molecular weight of the lower band, consistent with core deglycosylation of pendrin. Conversely, upon treatment with N glycosidase F, which removes all glycosides, the ~ 130 kDa band disappeared and the ~ 90 kDa band moved to the same lower molecular weight seen after endoglycosidase H treatment, which corresponds to the expected molecular weight of the non-glycosylated protein (**Figure 6B**). These results confirm that the higher molecular weight band is the complex glycoprotein and the lower band is the core glycosylated protein.

In silico analysis of mouse pendrin (NetNGlyc 1.0 Server) predicted five putative N-linked glycosylation sites at asparagines 167, 172, 241, 475 and 567. Site-directed mutagenesis, in which asparagine was substituted for alanine, showed that only the first two sites, N167 and N172, account for the full glycosylation of pendrin (**Figure 6B**).

We next evaluated the role of glycosylation on the membrane targeting, the polarization, and the activity of pendrin. These experiments were performed in OKP cells stably transfected with either wild type or N167A/N172A double mutant pendrin, because OKP cells exhibit a much higher transfection rate (up to 80%) compared to HEK293 cells, and they are polarized when grown on filters. **Figure 7A-C** shows that in polarized OKP cells (as in HEK293 cells; see **Figure 1**), wild type pendrin colocalized with biotin at the plasma membrane. Moreover, pendrin was preferentially expressed at the apical cell border (**Figure 7D**), as in native collect-

ing duct B-ICs. A similar pattern of apical membrane expression was observed with the N167A/N172A double mutant pendrin (**Figure 7E-H**).

Membrane expression of pendrin with disrupted N-linked glycosylation sites in stably transfected, non-polarized OKP cells was confirmed by cell surface biotinylation followed by avidin bead precipitation and immunoblotting. Results show that pendrin was expressed at a lesser level in cells expressing the N167A/N172A double mutant pendrin than in cells expressing the wild type pendrin, but the fraction of pendrin expressed at the cell surface was similar in the two cell lines (**Figure 8A**). Furthermore, the functional pendrin activity in these two OKP cell lines, as determined under the forward Cl^-/OH^- exchange mode at pH_e 7.4, was proportional to their expression level of pendrin at the cell surface (**Figure 8B**). However, in contrast to the wild type pendrin, the activity of which increases at low pH_e in OKP cells as in HEK293 cells, the activity of the N167A/N172A double mutant pendrin did not increase at pH_e 6.0 (**Figure 8B**).

Altogether these results indicate that glycosylation is not required for the expression of pendrin at the apical cell surface and its activity, but that it is a determinant of its sensitivity to external pH.

DISCUSSION

Pendrin has been shown to play a key role in maintaining the homeostasis of the inner ear [25] and in regulating the renal chloride balance [13, 14]; hence the importance of fully characterizing its structure and function. Pendrin expression in *Xenopus laevis* oocytes or in HEK293 cells previously demonstrated that it can function in several distinct modes including Cl^-/I^- , Cl^-/OH^- , $\text{Cl}^-/\text{HCO}_3^-$ and $\text{Cl}^-/\text{formate}$ exchange [22, 26], and that it is sensitive to DIDS [22]. In this study, we sought to characterize the glycosylation properties of pendrin, its kinetic behaviour, and its regulation by pH. Stable expression of mouse full-length pendrin in HEK293 cells enabled us to examine its function as a Cl^-/OH^- and $\text{Cl}^-/\text{HCO}_3^-$ reversible exchanger.

We found that the activity of pendrin was significantly higher in the $\text{Cl}^-/\text{HCO}_3^-$ exchange mode, that is, its predominant transport mode in the kidney collecting duct [27]. In rabbit CCD, Schuster [28] estimated the K_m for luminal chloride as 4-11 mM based upon his flux measurements, and as 1.7 mM based upon the fluxes reported in another study [29]. However, it is important to note that the K_m values measured in these previous studies are apparent trans-epithelial kinetic parameters and cannot be considered as true affinity constants in the enzymatic sense; the measured fluxes included a contribution by other transporters, such as basolateral anion exchangers. In contrast, our values were obtained in heterologous expression systems and reflected only the activity of pendrin. Moreover, they were corrected to account for variations in gradients and driving forces as external and/or internal concentrations were themselves varied. The apparent Cl^- affinity values that we measured (1.35 mM at $\text{pH}_i = 8.0$, 24 mM at $\text{pH}_i = 7.0$) are significantly lower than the true affinity values that we calculated (3 and 75 mM, respectively). From a physiological standpoint, the relatively high affinity of pendrin for external Cl^- at high pH values could play an important role in the kidney collecting duct: it would allow the exchanger to function at very low Cl^- concentrations and secrete bicarbonate in states of alkalosis.

The pendrin affinity values obtained in this study may also be compared to those that have been reported for the $\text{Cl}^-/\text{HCO}_3^-$ exchanger AE1. Based upon previously published experimental data [30, 31], Weinstein [24] calculated a K_m of 50 mM for Cl^- and 198 mM for HCO_3^- , with the assumption that internal and external affinities were equal. In a later study, Knauf et al. [32] estimated the true K_m of AE1 as 20 mM for external Cl^- (vs. 48 mM for internal Cl^-), and as 2 mM for external HCO_3^- (vs. 340 mM for internal HCO_3^-). These AE1 affinity values are comparable to those that we determined for pendrin at physiological pH values (i.e., $\text{pH}_i \sim 7.0$).

Importantly, we characterized the effect of intracellular (pH_i) and extracellular (pH_e) pH on the kinetics of the transporter. We measured pendrin activity at pH values varying from 6 to 8; note that during ischemic episodes, intracellular pH levels may drop as low as 6.2 [33]. Pendrin as a $\text{Cl}^-/\text{HCO}_3^-$ exchanger is known to contribute to the regulation of intracellular and extracellular pH [27]. Conversely, we established for the first time that pendrin is regulated by pH. More specifically, we found that pendrin activity *in vitro* is significantly higher at acid pH_e . Mathematical analysis of the fluxes showed that the effects of pH_e can be accounted for assuming that a low pH_e accelerates ion translocation, possibly via allosteric modifications. The effects of pH_i on pendrin kinetics could be explained by a pH_i -induced modification of binding affinities. The affinity of pendrin for Cl^- was predicted to increase by a factor of 25 as pH_i decreased from 8.0 to 7.0, whereas that for OH^- was reduced by a factor of 5.

The regulation of AE isoforms by pH was previously established by several investigators [34-36]. In particular, the study of Sterling and Casey [34] demonstrated that AE1 and AE3 isoforms are essentially insensitive to pH, whereas AE2 appears to be slightly inhibited by acid pH and more significantly activated by high pH. Although the latter findings would sug-

gest that pH exerts opposite effects on AE2 and pendrin, it should be noted that in contrast to our present measurements of pendrin activity, pH_i and pH_e were varied simultaneously in the study of Sterling and Casey; thus, we can not rule out the possibility that pH_i and pH_e exert inverse regulatory effects on AE2. Interpreting flux measurements for an acid-base transporter is complicated by the combined effect of ionic concentrations on the driving force and potential pH regulation sites. Our mathematical model enabled us to show that pH-mediated changes in pendrin activity were not due to variations in transmembrane gradients but to an intrinsic pH effect. In the kidney, the stimulating effect of low extracellular pH on pendrin activity suggests that the exchanger is constitutively activated, since urine is known to be acid. This may also be the case in the endolymphatic sac of the inner ear, where pendrin has been shown to contribute to pH buffering by secreting bicarbonate [37]. The endolymph is known to be acidic (pH ~ 6.6-7.1) [38-40], and endolymphatic pH homeostasis is necessary for the prevention of hearing loss. Thus, the constitutive stimulation of pendrin in the endolymphatic sac may represent an important regulation pathway in the inner ear.

Our results indicate that pendrin is glycosylated exclusively at asparagines 167 and 172, which are located in the second putative extracellular loop of pendrin. N-glycosylation of membrane proteins plays a role in their correct folding and their targeting to the membrane [41, 42]. Some studies also suggest that glycosylation may have a role in maintaining the transporter in an active form within the membrane [43, 44]. Hence, the role of N-glycosylation sites varies among different proteins. In contrast to the rat Na^+Cl^- thiazide-sensitive co-transporter (Slc12a3) which displays diminished surface expression and activity when its N-glycosylation sites are disrupted [43], N-glycosylation of pendrin does not appear to be a pre-requisite for its targeting to the cell surface and polarized expression at the apical cell border. Although N-glycosylation is not required for the basal transport activity of pendrin, mutation of the two N-glycosylated asparagines (Asn) to alanines (Ala) abrogates the external pH dependence of pendrin activity. Several hypotheses can be put forward to account for this effect: 1) the sugar residues are the proton sensor; however, to our knowledge, this has never been reported before; 2) the loss of the sugar residues modifies the conformation of the protein and masks the proton sensor; 3) the replacement of Asn by Ala modifies the conformation of the protein and masks the proton sensor, independently of the loss of the sugar residues; 4) mutated Asn are the proton sensor responsible for the modulation of pendrin activity. Further experiments are needed to address these hypotheses.

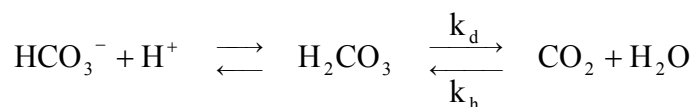
In summary, we characterized both experimentally and theoretically the kinetic behaviour of pendrin. We showed for the first time that pendrin activity is modulated by both internal and external pH, and that the dependence on external pH is lost by mutagenesis-induced disruption of N-glycosylation sites. The sensitivity of pendrin to pH may serve as a key mechanism in controlling ionic exchanges across the plasma membrane of type-B intercalated cells in the kidney collecting duct.

ACKNOWLEDGEMENTS

The authors are grateful to Kent A. Riemondy, University of Colorado, for providing the pendrin transfection plasmid.

Appendix A. Bicarbonate Concentration

Bicarbonate and carbonic acid form an acid/base pair. In water, carbonic acid and carbon dioxide are inter-converted:



where k_d and k_h are the H_2CO_3 dehydration and hydration rates, respectively taken as 18 and 0.037 s^{-1} [45]. We assume that the dissociation of H_2CO_3 is rapid and at equilibrium. Thus, the acid-base concentration ratio is given by:

$$\text{pH} = \text{pKa} + \log\left(\frac{[\text{HCO}_3^-]}{[\text{H}_2\text{CO}_3]}\right) \quad (1)$$

$$\text{That is, } [\text{H}_2\text{CO}_3] = [\text{HCO}_3^-] \times 10^{\text{pKa}-\text{pH}} \quad (2)$$

The temporal concentration variations can be written as:

$$\frac{d[\text{HCO}_3^-]}{dt} + \frac{d[\text{H}_2\text{CO}_3]}{dt} = -k_d[\text{HCO}_3^-] + k_h[\text{CO}_2] \quad (3)$$

$$\frac{d[\text{CO}_2]}{dt} = +k_d[\text{HCO}_3^-] - k_h[\text{CO}_2] \quad (4)$$

Adding Eqs. (3-4) yields:

$$\frac{d}{dt}([\text{HCO}_3^-] + [\text{H}_2\text{CO}_3] + [\text{CO}_2]) = 0 \quad (5)$$

$$[\text{HCO}_3^-] + [\text{H}_2\text{CO}_3] + [\text{CO}_2] = C_{\text{tot}} \quad (6)$$

where the constant C_{tot} is the total concentration of all bicarbonate species (i.e., $\text{HCO}_3^- + \text{H}_2\text{CO}_3 + \text{CO}_2$). Combining Eqs. (2) and (6), we obtain:

$$[\text{CO}_2] = C_{\text{tot}} - [\text{HCO}_3^-](1 + 10^{\text{pKa}-\text{pH}}) \quad (7)$$

Substituting Eqs. (2) and (7) into Eq. (3) and rearranging yields an equation for the time derivative of $[\text{HCO}_3^-]$ only:

$$\frac{d[\text{HCO}_3^-]}{dt} = -\left(\frac{k_d(10^{\text{pKa}-\text{pH}}) + k_h(1 + 10^{\text{pKa}-\text{pH}})}{(1 + 10^{\text{pKa}-\text{pH}})}\right)[\text{HCO}_3^-] + \left(\frac{k_h}{1 + 10^{\text{pKa}-\text{pH}}}\right)C_{\text{tot}} \quad (8)$$

$$\text{Let } k_1 \equiv \frac{k_d(10^{\text{pKa}-\text{pH}}) + k_h(1 + 10^{\text{pKa}-\text{pH}})}{(1 + 10^{\text{pKa}-\text{pH}})} \quad (9)$$

$$k_2 \equiv \frac{k_h}{k_d(10^{\text{pKa}-\text{pH}}) + k_h(1 + 10^{\text{pKa}-\text{pH}})}$$

Integration of Eq. (8) yields the concentration of bicarbonate as a function of time:

$$[\text{HCO}_3^-] = C_{\text{tot}}(k_2 + (1 - k_2)\exp(-k_1 t)) \quad (10)$$

In our experiments, the total concentration of bicarbonate species is equal to the initial concentration of HCO_3^- (denoted $[\text{HCO}_3^-]_0$). Equation (10) can therefore be expressed as:

$$\frac{[\text{HCO}_3^-]_t}{[\text{HCO}_3^-]_0} = k_2 + (1 - k_2)\exp(-k_1 t) \quad (11)$$

where the subscript “t” denotes any time t, and “o” the starting point of the experiment. As demonstrated by Eq. (11), the equilibrium (“eq”) concentration of HCO_3^- is:

$$\frac{[\text{HCO}_3^-]_{\text{eq}}}{[\text{HCO}_3^-]_0} = k_2 = \frac{0.037}{18(10^{3.57-7.40}) + 0.037(1 + 10^{3.57-7.40})} = 0.9327 \quad (12)$$

That is, HCO_3^- concentration at equilibrium is 6.73% lower than that at the starting point. Given that $\exp(-3) = 0.05$, we can also estimate the time needed to reach 95% of the equilibrium concentration (t_{95}) as:

$$t_{95} = \frac{3}{k_1} = \frac{3(1 + 10^{3.57-7.40})}{18(10^{3.57-7.40}) + 0.037(1 + 10^{3.57-7.40})} = 75.64 \text{ s} \quad (13)$$

Appendix B. Kinetic Parameter Evaluation

As depicted on **Figure 5**, the transport of a given species (e.g., Cl^- , HCO_3^- , or OH^-) across pendrin is characterized by 4 parameters: the external and internal binding constants (K^e, K^i) and the forward and backward translocation rates (P^e, P^i), where the superscripts “e” and “i” respectively denote the extracellular and intracellular compartments. The non-dimensional external and internal concentrations of chloride (γ), bicarbonate (β), and OH^- (α) are defined as:

$$\gamma^e = \frac{[\text{Cl}^-]^e}{K_{\text{Cl}}^e}, \gamma^i = \frac{[\text{Cl}^-]^i}{K_{\text{Cl}}^i} \quad (14a)$$

$$\beta^e = \frac{[\text{HCO}_3^-]^e}{K_{\text{HCO}_3}^e}, \beta^i = \frac{[\text{HCO}_3^-]^i}{K_{\text{HCO}_3}^i} \quad (14b)$$

$$\alpha^e = \frac{[\text{OH}^-]^e}{K_{\text{OH}}^e}, \alpha^i = \frac{[\text{OH}^-]^i}{K_{\text{OH}}^i} \quad (14c)$$

General Equations

Following the approach of Weinstein [46], we assume that anion binding occurs much faster than translocation, so that the concentration of bound carrier on each side is calculated based on the equilibrium binding constants. Thus, if x^e and x^i respectively denote the concentration of unloaded carrier on the external and internal sides, the concentration of carrier bound to Cl^- on the external and internal sides is calculated as $\gamma^e x^e$ and $\gamma^i x^i$, respectively. Similarly, the concentration of carrier bound to HCO_3^- and OH^- is given by $\beta^e x^e$ and $\alpha^e x^e$ on the external side, and by $\beta^i x^i$ and $\alpha^i x^i$ on the internal side. If x_{total} represents the density of total carrier, conservation of total carrier can then be written as:

$$(1 + \gamma^e + \beta^e + \alpha^e)x^e + (1 + \gamma^i + \beta^i + \alpha^i)x^i = x_{\text{total}} \quad (15)$$

That is, $\delta^e x^e + \delta^i x^i = x_{\text{total}}$ (16)

where: $\delta^e \equiv (1 + \gamma^e + \beta^e + \alpha^e)$
 $\delta^i \equiv (1 + \gamma^i + \beta^i + \alpha^i)$

In addition, there is no net flux of loaded and unloaded carrier across the membrane, so that:

$$(P_{\text{Cl}}^e \gamma^e + P_{\text{HCO}_3}^e \beta^e + P_{\text{OH}}^e \alpha^e)x^e = (P_{\text{Cl}}^i \gamma^i + P_{\text{HCO}_3}^i \beta^i + P_{\text{OH}}^i \alpha^i)x^i \quad (17)$$

That is, $\eta^e x^e = \eta^i x^i$ (18)

where: $\eta^e \equiv (P_{\text{Cl}}^e \gamma^e + P_{\text{HCO}_3}^e \beta^e + P_{\text{OH}}^e \alpha^e)$
 $\eta^i \equiv (P_{\text{Cl}}^i \gamma^i + P_{\text{HCO}_3}^i \beta^i + P_{\text{OH}}^i \alpha^i)$

Substituting Eq. (18) into (16) yields:

$$x^e = x_{\text{total}} \eta^i / \sigma \quad (19a)$$

$$x^i = x_{\text{total}} \eta^e / \sigma \quad (19b)$$

where: $\sigma \equiv \delta^e \eta^i + \delta^i \eta^e$

The net fluxes of Cl^- , HCO_3^- and OH^- into the cell can then be calculated as:

$$J_{\text{Cl}}^{\text{net}} = J_{\text{Cl}}^{\text{influx}} - J_{\text{Cl}}^{\text{efflux}} = P_{\text{Cl}}^e \gamma^e x^e - P_{\text{Cl}}^i \gamma^i x^i = x_{\text{total}} \left(\frac{P_{\text{Cl}}^e \gamma^e \eta^i - P_{\text{Cl}}^i \gamma^i \eta^e}{\sigma} \right) \quad (20a)$$

$$J_{\text{HCO}_3}^{\text{net}} = J_{\text{HCO}_3}^{\text{influx}} - J_{\text{HCO}_3}^{\text{efflux}} = P_{\text{HCO}_3}^e \beta^e x^e - P_{\text{HCO}_3}^i \beta^i x^i = x_{\text{total}} \left(\frac{P_{\text{HCO}_3}^e \beta^e \eta^i - P_{\text{HCO}_3}^i \beta^i \eta^e}{\sigma} \right) \quad (20b)$$

$$J_{\text{OH}}^{\text{net}} = J_{\text{OH}}^{\text{influx}} - J_{\text{OH}}^{\text{efflux}} = P_{\text{OH}}^e \alpha^e x^e - P_{\text{OH}}^i \alpha^i x^i = x_{\text{total}} \left(\frac{P_{\text{OH}}^e \alpha^e \eta^i - P_{\text{OH}}^i \alpha^i \eta^e}{\sigma} \right) \quad (20c)$$

Cl/OH exchange: Cl influx

In the first set of Cl/OH⁻ exchange experiments, the dpH/dt variations are proportional to the efflux of OH⁻. Before addition of Cl⁻ to the bath at t = 0, the intracellular concentration of Cl⁻ is negligible. Thus, we assume that $\gamma^i \sim 0$ immediately after t = 0. In addition, there is no bicarbonate (i.e., $\beta^i = \beta^e = 0$). Under these conditions, Eq. (20c) yields the OH⁻ efflux as:

$$J_{\text{OH}}^{\text{efflux}} = \frac{x_{\text{total}} P_{\text{OH}}^i \alpha^i P_{\text{Cl}}^e \gamma^e}{\gamma^e [P_{\text{OH}}^i \alpha^i + P_{\text{Cl}}^e (1 + \alpha^i)] + P_{\text{OH}}^i \alpha^i (1 + \alpha^e) + P_{\text{OH}}^e \alpha^e (1 + \alpha^i)} \quad (21)$$

After rearrangement, the flux can be rewritten as:

$$J_{\text{OH}}^{\text{efflux}} = \left[\frac{x_{\text{total}} P_{\text{OH}}^i P_{\text{Cl}}^e}{P_{\text{OH}}^i + P_{\text{Cl}}^e (1 + 1/\alpha^i)} \right] \frac{\gamma^e}{\gamma^e + \frac{P_{\text{OH}}^i (1 + \alpha^e) + P_{\text{OH}}^e \alpha^e (1 + 1/\alpha^i)}{P_{\text{OH}}^i + P_{\text{Cl}}^e (1 + 1/\alpha^i)}} \quad (22)$$

In other words,

$$J_{\text{OH}}^{\text{efflux}} = J_{\text{OH}}^{\text{efflux,max}} \frac{[\text{Cl}^-]^e}{[\text{Cl}^-]^e + K_{\text{Cl}}^{\text{e,app}}}, \quad (23a)$$

where the maximal flux and apparent affinity are given by:

$$J_{\text{OH}}^{\text{efflux,max}} = \left[\frac{x_{\text{total}} P_{\text{OH}}^i P_{\text{Cl}}^e}{P_{\text{OH}}^i + P_{\text{Cl}}^e (1 + 1/\alpha^i)} \right] \quad (23b)$$

$$K_{\text{Cl}}^{\text{e,app}} = K_{\text{Cl}}^e \left(\frac{P_{\text{OH}}^i (1 + \alpha^e) + P_{\text{OH}}^e \alpha^e (1 + 1/\alpha^i)}{P_{\text{OH}}^i + P_{\text{Cl}}^e (1 + 1/\alpha^i)} \right) \quad (23c)$$

Note that Eq. (23) represents a Michaelis-Menten relationship, in accordance with the kinetic curve shown in **Figure 4A**.

Cl/OH exchange: Cl efflux

In the second set of experiments, the the dpH_i/dt variations are proportional to the influx of OH^- . By symmetry with the preceding set of experiments, we have:

$$J_{OH}^{inf\ lux} = J_{OH}^{inf\ lux, max} \frac{[Cl^-]^e}{[Cl^-]^e + K_{Cl}^{i, app}}, \quad (24a)$$

where the maximal flux and apparent affinity are given by:

$$J_{OH}^{inf\ lux, max} = \left[\frac{x_{total} P_{OH}^e P_{Cl}^i}{P_{OH}^e + P_{Cl}^i (1 + 1/\alpha^e)} \right] \quad (24b)$$

$$K_{Cl}^{i, app} = K_{Cl}^i \left(\frac{P_{OH}^e (1 + \alpha^i) + P_{OH}^i \alpha^i (1 + 1/\alpha^e)}{P_{OH}^e + P_{Cl}^i (1 + 1/\alpha^e)} \right) \quad (24c)$$

Cl⁻/HCO₃⁻ exchange

In the Cl^-/HCO_3^- exchange experiments, the dpH_i/dt variations are proportional to the net flux of HCO_3^- into the cell; it can be shown that the net flux of OH^- is negligible in comparison. Before addition of HCO_3^- to the bath at $t = 0$, the intracellular concentration of HCO_3^- is negligible. Under these conditions, immediately after $t = 0$, $\beta^i \sim 0$ and there is no HCO_3^- efflux. The flux of HCO_3^- into the cell is given by:

$$J_{HCO_3}^{inf\ lux} = \frac{x_{total} P_{HCO_3}^e \beta^e P_{Cl}^i \gamma^i}{\beta^e [P_{Cl}^i \gamma^i + P_{HCO_3}^e (1 + \gamma^i)] + P_{Cl}^i \gamma^i (1 + \gamma^e) + P_{HCO_3}^e \gamma^e (1 + \gamma^i)} \quad (25)$$

Rearranging Eq. 25 yields:

$$J_{HCO_3}^{inf\ lux} = \left[\frac{x_{total} P_{Cl}^i P_{HCO_3}^e}{[P_{Cl}^i + P_{HCO_3}^e (1 + 1/\gamma^i)]} \right] \frac{\beta^e}{\beta^e + \frac{P_{Cl}^i (1 + \gamma^e) + P_{Cl}^e \gamma^e (1 + 1/\gamma^i)}{[P_{Cl}^i + P_{HCO_3}^e (1 + 1/\gamma^i)]}} \quad (26)$$

Thus, the HCO_3^- influx can be expressed as:

$$J_{HCO_3}^{inf\ lux} = J_{HCO_3}^{inf\ lux, max} \frac{[HCO_3^-]^e}{[HCO_3^-]^e + K_{HCO_3}^{e, app}} \quad (27a)$$

where the maximal flux and apparent affinity are given by:

$$J_{HCO_3}^{inf\ lux, max} = \left[\frac{x_{total} P_{Cl}^i P_{HCO_3}^e}{[P_{Cl}^i + P_{HCO_3}^e (1 + 1/\gamma^i)]} \right] \quad (27b)$$

$$K_{HCO_3}^{e, app} = K_{HCO_3}^e \left(\frac{P_{Cl}^i (1 + \gamma^e) + P_{Cl}^e \gamma^e (1 + 1/\gamma^i)}{[P_{Cl}^i + P_{HCO_3}^e (1 + 1/\gamma^i)]} \right) \quad (27c)$$

Parameter Fit

For the 3 species considered here, there is a total of $4 \times 3 = 12$ parameters (notwithstanding the total carrier density x_{total} , which is not an intrinsic property of pendrin). However, these parameters are not all independent; since there is no net flux across the exchanger when external and internal concentrations are equal, we have:

$$\frac{P_{\text{Cl}}^e K_{\text{Cl}}^i}{K_{\text{Cl}}^e P_{\text{Cl}}^i} = \frac{P_{\text{HCO}_3}^e K_{\text{HCO}_3}^i}{K_{\text{HCO}_3}^e P_{\text{HCO}_3}^i} = \frac{P_{\text{OH}}^e K_{\text{OH}}^i}{K_{\text{OH}}^e P_{\text{OH}}^i} \quad (28)$$

Thus, the number of independent parameters (in addition to x_{total}) is 10. As shown in Eqs. (23, 24, 27), the 3 maximum fluxes and the apparent external affinities for HCO_3^- and Cl^- are constant in each set of experiments, that is, they do not depend on variable concentrations. In contrast, the apparent internal affinity for Cl^- (Eq. 24c) is a function of the intracellular pH (i.e., α^i) which is variable. This means that our experiments can yield a total of 6 parameters, and that the others have to be assumed. We therefore assumed that the internal and external binding affinities of a given ion are equal, as is usually done [46], and we fixed the forward Cl^- translocation rate (P_{Cl}^e). The remaining 6 parameters were fitted to the data shown in **Figures 4A-C** using the non-linear data fitting optimization procedure `lsqnonlin` on Matlab®.

The forward Cl^- translocation rate (P_{Cl}^e) was varied between 10^{+2} s^{-1} (i.e., the turnover rate for the $\text{Na}^+ \text{-K}^+ \text{-ATPase}$) and 10^{+6} s^{-1} (i.e., that of an ion channel) [46]. For each value of P_{Cl}^e , the remaining six parameters were fitted to the experimental data. The error function was the same in all cases, and the affinity values and the ratios of the translocation rates to P_{Cl}^e were found to be almost insensitive to the value of P_{Cl}^e . The value of P_{Cl}^e was then fixed at 10^{+4} s^{-1} , a mid-range value. The fitted parameter values corresponding to $P_{\text{Cl}}^e = 10^{+4} \text{ s}^{-1}$ are shown in **Table 1**.

Accepted Manuscript

REFERENCES

- 1 Reardon, W. and Trembath, R. C. (1996) Pendred syndrome. *J Med Genet.* **33**, 1037-1040
- 2 Kraiem, Z., Heinrich, R., Sadeh, O., Shiloni, E., Nassir, E., Hazani, E. and Glaser, B. (1999) Sulfate transport is not Impaired in Pendred syndrome thyrocytes. *J Clin Endocrinol Metab.* **84**, 2574-2576
- 3 Royaux, I. E., Suzuki, K., Mori, A., Katoh, R., Everett, L. A., Kohn, L. D. and Green, E. D. (2000) Pendrin, the protein encoded by the Pendred syndrome gene (PDS), is an apical porter of iodide in the thyroid and is regulated by thyroglobulin in FRTL-5 cells. *Endocrinology.* **141**, 839-845
- 4 Scott, D. A. and Karniski, L. P. (2000) Human pendrin expressed in *Xenopus laevis* oocytes mediates chloride/formate exchange. *Am J Physiol Cell Physiol.* **278**, C207-211
- 5 Kopp, P., Pesce, L. and Solis-S, J. C. (2008) Pendred syndrome and iodide transport in the thyroid. *Trends Endocrinol Metab.* **19**, 260-268
- 6 Maciaszczyk, L. and Lewinski, A. (2008) Phenotypes of SLC26A4 gene mutations: Pendred syndrome and hypoacusis with enlarged vestibular aqueduct. *Neuro Endocrinol Lett.* **29**, 29-36
- 7 Rillema, J. A. and Hill, M. A. (2003) Prolactin regulation of the pendrin-iodide transporter in the mammary gland. *Am J Physiol Endocrinol Metab.* **284**, E25-28
- 8 Suzuki, K., Royaux, I. E., Everett, L. A., Mori-Aoki, A., Suzuki, S., Nakamura, K., Sakai, T., Katoh, R., Toda, S., Green, E. D. and Kohn, L. D. (2002) Expression of PDS/Pds, the Pendred syndrome gene, in endometrium. *J Clin Endocrinol Metab.* **87**, 938
- 9 Bidart, J.-M., Lacroix, L., Evain-Brion, D., Caillou, B., Lazar, V., Frydman, R., Bellet, D., Filetti, S. and Schlumberger, M. (2000) Expression of Na⁺/I⁻ symporter and Pendred syndrome genes in trophoblast cells. *J Clin Endocrinol Metab.* **85**, 4367-4372
- 10 Royaux, I. E., Wall, S. M., Karniski, L. P., Everett, L. A., Suzuki, K., Knepper, M. A. and Green, E. D. (2001) Pendrin, encoded by the Pendred syndrome gene, resides in the apical region of renal intercalated cells and mediates bicarbonate secretion. *Proceedings of the National Academy of Sciences of the United States of America.* **98**, 4221-4226
- 11 Wall, S. M., Kim, Y. H., Stanley, L., Glapion, D. M., Everett, L. A., Green, E. D. and Verlander, J. W. (2004) NaCl restriction upregulates renal Slc26a4 through subcellular redistribution: Role in Cl⁻ conservation. *Hypertension.* **44**, 982-987
- 12 Verlander, J. W., Hassell, K. A., Royaux, I. E., Glapion, D. M., Wang, M.-E., Everett, L. A., Green, E. D. and Wall, S. M. (2003) Deoxycorticosterone upregulates PDS (Slc26a4) in mouse kidney: Role of pendrin in mineralocorticoid-induced hypertension. *Hypertension.* **42**, 356-362
- 13 Quentin, F., Chambrey, R., Trinh-Trang-Tan, M. M., Fysekidis, M., Cambillau, M., Paillard, M., Aronson, P. S. and Eladari, D. (2004) The Cl⁻/HCO₃⁻ exchanger pendrin in the rat kidney is regulated in response to chronic alterations in chloride balance. *Am J Physiol Renal Physiol.* **287**, F1179-1188
- 14 Vallet, M., Picard, N., Loffing-Cueni, D., Fysekidis, M., Bloch-Faure, M., Deschenes, G., Breton, S., Meneton, P., Loffing, J., Aronson, P. S., Chambrey, R. and Eladari, D. (2006) Pendrin regulation in mouse kidney primarily is chloride-dependent. *J Am Soc Nephrol.* **17**, 2153-2163
- 15 Leviel, F., Hubner, C. A., Houillier, P., Morla, L., El Moghrabi, S., Brideau, G., Hatim, H., Parker, M. D., Kurth, I., Kougioumtzes, A., Sinning, A., Pech, V., Riemondy, K. A., Miller, R. L., Hummler, E., Shull, G. E., Aronson, P. S., Doucet, A., Wall, S. M., Chambrey, R. and Eladari, D. (2010) The Na⁺-dependent chloride-bicarbonate exchanger SLC4A8

- mediates an electroneutral Na⁺ reabsorption process in the renal cortical collecting ducts of mice. *The Journal of Clinical Investigation*. **120**, 1627-1635
- 16 Kahle, K. T., Gimenez, I., Hassan, H., Wilson, F. H., Wong, R. D., Forbush, B., Aronson, P. S. and Lifton, R. P. (2004) WNK4 regulates apical and basolateral Cl⁻ flux in extrarenal epithelia. *Proceedings of the National Academy of Sciences of the United States of America*. **101**, 2064-2069
- 17 Schambelan, M., Sebastian, A. and Rector, F. C., Jr. (1981) Mineralocorticoid-resistant renal hyperkalemia without salt wasting (type II pseudohypoaldosteronism): Role of increased renal chloride reabsorption. *Kidney Int*. **19**, 716-727
- 18 Take, C., Ikeda, K., Kurasawa, T. and Kurokawa, K. (1991) Increased chloride reabsorption as an inherited renal tubular defect in familial type II pseudohypoaldosteronism. *New England Journal of Medicine*. **324**, 472-476
- 19 Yamauchi, K., Rai, T., Kobayashi, K., Sohara, E., Suzuki, T., Itoh, T., Suda, S., Hayama, A., Sasaki, S. and Uchida, S. (2004) Disease-causing mutant WNK4 increases paracellular chloride permeability and phosphorylates claudins. *Proceedings of the National Academy of Sciences of the United States of America*. **101**, 4690-4694
- 20 Wagner, C. A., Finberg, K. E., Stehberger, P. A., Lifton, R. P., Giebisch, G. H., Aronson, P. S. and Geibel, J. P. (2002) Regulation of the expression of the Cl⁻/anion exchanger pendrin in mouse kidney by acid-base status. *Kidney Int*. **62**, 2109-2117
- 21 Knauf, F., Yang, C.-L., Thomson, R. B., Mentone, S. A., Giebisch, G. and Aronson, P. S. (2001) Identification of a chloride-formate exchanger expressed on the brush border membrane of renal proximal tubule cells. *Proceedings of the National Academy of Sciences of the United States of America*. **98**, 9425-9430
- 22 Soleimani, M., Greeley, T., Petrovic, S., Wang, Z., Amlal, H., Kopp, P. and Burnham, C. E. (2001) Pendrin: an apical Cl⁻/OH⁻/HCO₃⁻ exchanger in the kidney cortex. *Am J Physiol Renal Physiol*. **280**, F356-364
- 23 Shcheynikov, N., Yang, D., Wang, Y., Zeng, W., Karniski, L. P., So, I., Wall, S. M. and Muallem, S. (2008) The Slc26a4 transporter functions as an electroneutral Cl⁻/I⁻/HCO₃⁻ exchanger: role of Slc26a4 and Slc26a6 in I⁻ and HCO₃⁻ secretion and in regulation of CFTR in the parotid duct. *The Journal of Physiology*. **586**, 3813-3824
- 24 Weinstein, A. M. (2000) A mathematical model of the outer medullary collecting duct of the rat. *Am J Physiol Renal Physiol*. **279**, F24-45
- 25 Royaux, I., Belyantseva, I., Wu, T., Kachar, B., Everett, L., Marcus, D. and Green, E. (2003) Localization and functional studies of pendrin in the mouse inner ear provide insight about the etiology of deafness in Pendred syndrome. *JARO - Journal of the Association for Research in Otolaryngology*. **4**, 394-404
- 26 Scott, D. A., Wang, R., Kreman, T. M., Scheffield, V. C. and Karniski, L. P. (1999) The Pendred syndrome gene encodes a chloride-iodide transport protein. *Nature Genetics*. **21**, 440-443
- 27 Schuster, V. L. (1991) Cortical collecting duct bicarbonate secretion. *Kidney Int Suppl*. **33**, S47-S50
- 28 Schuster, V. L. (1986) Cyclic adenosine monophosphate-stimulated anion transport in rabbit cortical collecting duct. Kinetics, stoichiometry, and conductive pathways. *The Journal of Clinical Investigation*. **78**, 1621-1630
- 29 Garcia-Austt, J., Good, D. W., Burg, M. B. and Knepper, M. A. (1985) Deoxycorticosterone-stimulated bicarbonate secretion in rabbit cortical collecting ducts: effects of luminal chloride removal and in vivo acid loading. *Am J Physiol Renal Physiol*. **249**, F205-212
- 30 Gasbjerg, P. K., Knauf, P. A. and Brahm, J. (1996) Kinetics of bicarbonate transport in human red blood cell membranes at body temperature. *The Journal of General Physiology*. **108**, 565-575

- 31 Knauf, P. A., Gasbjerg, P. K. and Brahm, J. (1996) The asymmetry of chloride transport at 38 degrees C in human red blood cell membranes. *The Journal of General Physiology*. **108**, 577-589
- 32 Knauf, P. A., Law, F.-Y., Leung, T.-W. V., Gehret, A. U. and Perez, M. L. (2002) Substrate-dependent reversal of anion transport site orientation in the human red blood cell anion-exchange protein, AE1. *Proceedings of the National Academy of Sciences of the United States of America*. **99**, 10861-10864
- 33 Garlick, P. B., Radda, G. K. and Seeley, P. J. (1979) Studies of acidosis in the ischaemic heart by phosphorus nuclear magnetic resonance. *Biochem J*. **184**, 547-554
- 34 Sterling, D. and Casey, J. R. (1999) Transport activity of AE3 chloride/bicarbonate anion-exchanger proteins and their regulation by intracellular pH. *Biochem J*. **344**, 221-229
- 35 Humphreys, B. D., Jiang, L., Chernova, M. N. and Alper, S. L. (1994) Functional characterization and regulation by pH of murine AE2 anion exchanger expressed in *Xenopus* oocytes. *Am J Physiol Cell Physiol*. **267**, C1295-1307
- 36 Zhang, Y., Chernova, M. N., Stuart-Tilley, A. K., Jiang, L. and Alper, S. L. (1996) The cytoplasmic and transmembrane domains of AE2 both contribute to regulation of anion exchange by pH. *Journal of Biological Chemistry*. **271**, 5741-5749
- 37 Wangemann, P., Nakaya, K., Wu, T., Maganti, R. J., Itza, E. M., Sanneman, J. D., Harbidge, D. G., Billings, S. and Marcus, D. C. (2007) Loss of cochlear HCO₃⁻ secretion causes deafness via endolymphatic acidification and inhibition of Ca²⁺ reabsorption in a Pendred syndrome mouse model. *Am J Physiol Renal Physiol*. **292**, F1345-1353
- 38 Everett, L. A., Morsli, H., Wu, D. K. and Green, E. D. (1999) Expression pattern of the mouse ortholog of the Pendred's syndrome gene (*Pds*) suggests a key role for pendrin in the inner ear. *Proceedings of the National Academy of Sciences of the United States of America*. **96**, 9727-9732
- 39 Couloigner, V., Teixeira, M., Hulin, P., Sterkers, O., Bichara, M., Escoubet, B., Planelles, G. and Ferrary, E. (2000) Effect of locally applied drugs on the pH of luminal fluid in the endolymphatic sac of guinea pig. *Am J Physiol Regul Integr Comp Physiol*. **279**, R1695-1700
- 40 Tsujikawa, S., Yamashita, T., Amano, H., Kumazawa, T. and Vosteen, K. H. (1992) Acidity in the endolymphatic sac fluid of guinea pigs. *ORL J Otorhinolaryngol Relat Spec*. **54**, 198-200
- 41 Asano, T., Takata, K., Katagiri, H., Ishihara, H., Inukai, K., Anai, M., Hirano, H., Yazaki, Y. and Oka, Y. (1993) The role of N-glycosylation in the targeting and stability of GLUT1 glucose transporter. *FEBS Letters*. **324**, 258-261
- 42 Fishburn, C. S., Elazar, Z. and Fuchs, S. (1995) Differential glycosylation and intracellular trafficking for the long and short isoforms of the D dopamine receptor. *Journal of Biological Chemistry*. **270**, 29819-29824
- 43 Hoover, R. S., Poch, E., Monroy, A., Vazquez, N., Nishio, T., Gamba, G. and Hebert, S. C. (2003) N-Glycosylation at two sites critically alters thiazide binding and activity of the rat thiazide-sensitive Na⁺:Cl⁻ cotransporter. *J Am Soc Nephrol*. **14**, 271-282
- 44 Paredes, A., Plata, C., Rivera, M., Moreno, E., Vazquez, N., Munoz-Clares, R., Hebert, S. C. and Gamba, G. (2006) Activity of the renal Na⁺-K⁺-2Cl⁻ cotransporter is reduced by mutagenesis of N-glycosylation sites: role for protein surface charge in Cl⁻ transport. *Am J Physiol Renal Physiol*. **290**, F1094-1102
- 45 Pocker, Y. and Bjorkquist, D. W. (1977) Stopped-flow studies of carbon dioxide hydration and bicarbonate dehydration in water and water-d₂. Acid-base and metal ion catalysis. *Journal of the American Chemical Society*. **99**, 6537-6543
- 46 Weinstein, A. M. (2010) A mathematical model of rat ascending Henle limb. I. Cotransporter function. *Am J Physiol Renal Physiol*. **298**, F512-524

FIGURE LEGENDS

Fig. 1. Immunolocalization of pendrin in stably transfected HEK293 cells. Confluent HEK293 cells transfected with pendrin were biotinylated and then stained for surface biotin (**A**, streptavidin-Cy5), nucleus (**B**, 4,6-diamidino 2-phenylindole dihydrochloride), and pendrin (**C**, anti-pendrin antibody followed by FITC-conjugated goat anti-rabbit IgG). The stained slides were visualized by confocal microscopy. **D** shows the merge of the three labelings.

Fig. 2. Representative traces showing pendrin-mediated changes in intracellular pH. Changes in pH_i in pendrin-transfected (black traces) or non-transfected (grey traces) HEK293 cells were induced by modifying the composition of the extracellular medium, as shown on top of each diagram. The initial rate of pH_i variation was determined over the first 20 sec period. The insets illustrate the transport mode of pendrin in each condition. In the absence of bicarbonate, pendrin was studied either under forward (**A**) or backward (**B**) Cl^-/OH^- exchange mode. In the presence of bicarbonate, it was measured under forward $\text{Cl}^-/\text{HCO}_3^-$ exchange mode (**C**).

Fig. 3. pH dependence of pendrin activity. **A.** After pre-incubation in a Cl^- -free medium at pH 7.4, cells were exposed to a medium containing 120 mM Cl^- at different pH values, and the initial rate of intracellular acidification was monitored. **B.** Cells were first incubated in a medium containing 120 mM Cl^- at pH 6.0, 7.4 or 8.0. After equilibration of intracellular pH, at 6.2, 7.0 and 7.5 respectively, cells were exposed to a Cl^- -free medium at pH 8.0, and the initial rate of intracellular alkalinisation was measured.

Fig. 4. Pendrin activity as a function of anion concentration. Pendrin activity was measured (black squares) as described in Figure 3 in the presence of different concentrations of Cl^- , OH^- and HCO_3^- . Also displayed are calculated values (white squares), computed using the mathematical model of pendrin-mediated ion transport. Insets show the Lineweaver-Burk plots of the measured data.

Fig. 5. Kinetic scheme of pendrin. Pendrin-mediated ion transport across the cell membrane is represented according to a ping-pong mechanism. Pd° and Pd^* refer to the free and ion-bound forms of pendrin, and P_{Cl} and P_{HCO_3} are the translocation rates of chloride and bicarbonate respectively (see Appendix B for details).

Fig. 6. Glycosylation of pendrin. **A.** Electrophoretical profile of pendrin in HEK293 cells transiently transfected with pendrin, in the absence of treatment or after treatment with endoglycosidase H, N glycosidase F, or sham treatment. Note that non-transfected cells display a non specific band at ~ 130 kDa. **B.** Electrophoretical profile of HEK293 cells transiently transfected with wild type pendrin (WT), or mutated pendrin with disruption of either only N167 or both N167 and N172 glycosylation sites.

Fig. 7. Immunolocalization of pendrin in stably transfected OKP cells. Confluent OKP cells stably transfected with either wild type (**A-D**) or N167A/N172A double mutant pendrin (**E-H**) were biotinylated and then stained for surface biotin (**A & E**, streptavidin-Cy5) and pendrin (**B & F**, anti-pendrin antibody followed by FITC-conjugated goat anti-rabbit IgG).

The stained slides were visualized by confocal microscopy. **C & G** show the merges of the two labellings. **D & H** show *x-z* reconstructions of confocal microscopy merge image stacks.

Fig. 8. Membrane expression and activity of pendrin with disrupted N-linked glycosylation sites. **A.** Pendrin immunoblot of biotinylated and whole cell proteins in OKP cells stably transfected with either wild type or N167A/N172A double mutant pendrin. The upper panel shows the blot and the lower panel shows the densitometry measurements of all the bands in each lane. **B.** Pendrin activity, measured under forward Cl^-/OH^- exchange mode at different external pH values (6.0, 7.4, and 8.0) in OKP cells stably transfected with either wild type or N167A/N172A double mutant pendrin. Values are means \pm SE from 6-9 samples in 2-3 experiments.

Accepted Manuscript

Table 1
Pendrin kinetic parameters

Ratio of Cl ⁻ backward rate to Cl ⁻ forward rate, P_{Cl}^i/P_{Cl}^e	1.239
Ratio of HCO ₃ ⁻ forward rate to Cl ⁻ forward rate $P_{HCO_3}^e/P_{Cl}^e$	10.76
Ratio of OH ⁻ forward rate to Cl ⁻ forward rate, P_{OH}^e/P_{Cl}^e	0.262
Cl ⁻ affinity, K_{Cl}	3.0 mM (pH _i = 8.0) 75 mM (pH _i = 7.0)
HCO ₃ ⁻ affinity, K_{HCO_3}	5.9 mM (pH _i = 7.2)
OH ⁻ affinity, K_{OH}	1.38x10 ⁻⁶ M (pH _i = 8.0) 2.62x10 ⁻⁷ M (pH _i = 7.0)

The parameters were fitted to the data shown in **Figure 4**, and correspond to an external pH of 7.4. The Cl⁻ forward rate (P_{Cl}^e) was fixed at 10,000 s⁻¹; the ratios of the other rates to P_{Cl}^e were found to be independent of its value. Note that the HCO₃⁻ and OH⁻ backward rates are not independent parameters; they can be obtained by using Eq. (28).

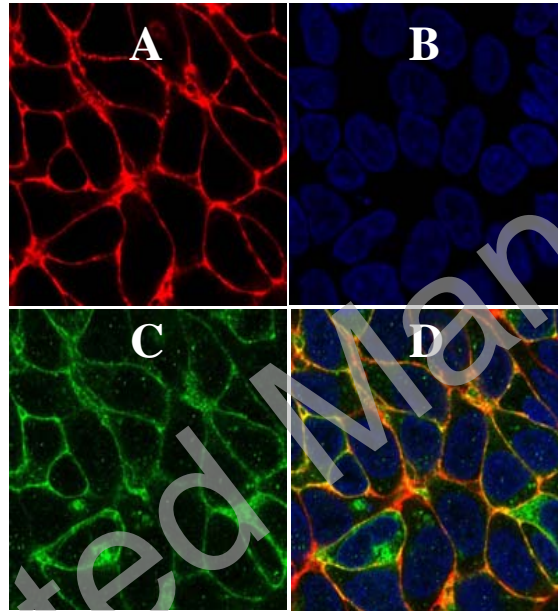


Figure 1. Immunolocalization of pendrin in stably transfected HEK293 cells.

Confluent HEK293 cells transfected with pendrin were biotinylated and then stained for surface biotin (**A**, streptavidin-Cy5), nucleus (**B**, 4,6-diamidino 2-phenylindole dihydrochloride), and pendrin (**C**, anti-pendrin antibody followed by FITC-conjugated goat anti-rabbit IgG). The stained slides were visualized by confocal microscopy. **D** shows the merge of the three labellings.

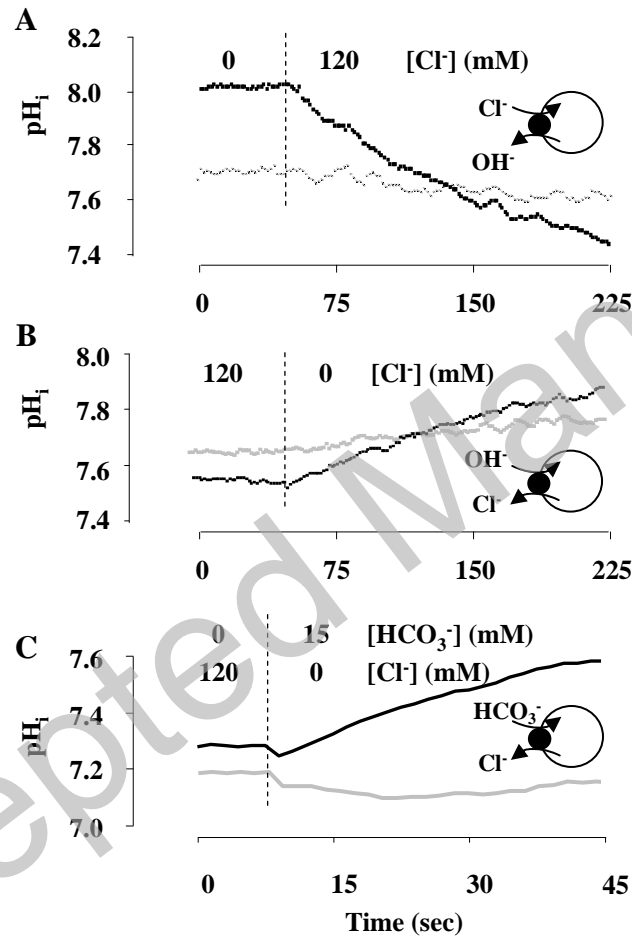


Figure 2. Representative traces showing pendrin-mediated changes in intracellular pH.

Changes in pH_i in pendrin-transfected (black traces) or non-transfected (grey traces) HEK cells were induced by modifying the composition of the extracellular medium, as shown on top of each diagram. The initial rate of pH_i variation was determined over the first 20 sec period. The insets illustrate the transport mode of pendrin in each condition. In the absence of bicarbonate, pendrin was studied either under forward (A) or backward (B) Cl^-/OH^- exchange mode. In the presence of bicarbonate, it was measured under forward Cl^-/HCO_3^- exchange mode (C).

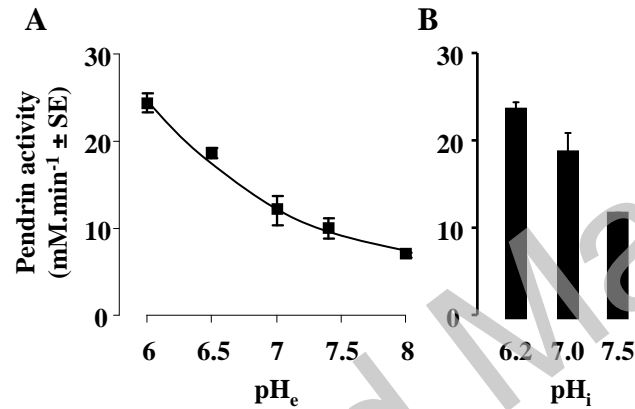


Figure 3. pH dependence of pendrin activity.

- A. After pre-incubation in a Cl⁻-free medium at pH 7.4, cells were exposed to a medium containing 120 mM Cl⁻ at different pH values, and the initial rate of intracellular acidification was monitored.
- B. Cells were first incubated in a medium containing 120 mM Cl⁻ at pH 6.0, 7.4 or 8.0. After equilibration of intracellular pH, at 6.2, 7.0 and 7.5 respectively, cells were exposed to a Cl⁻-free medium at pH 8.0, and the initial rate of intracellular alkalinisation was measured.

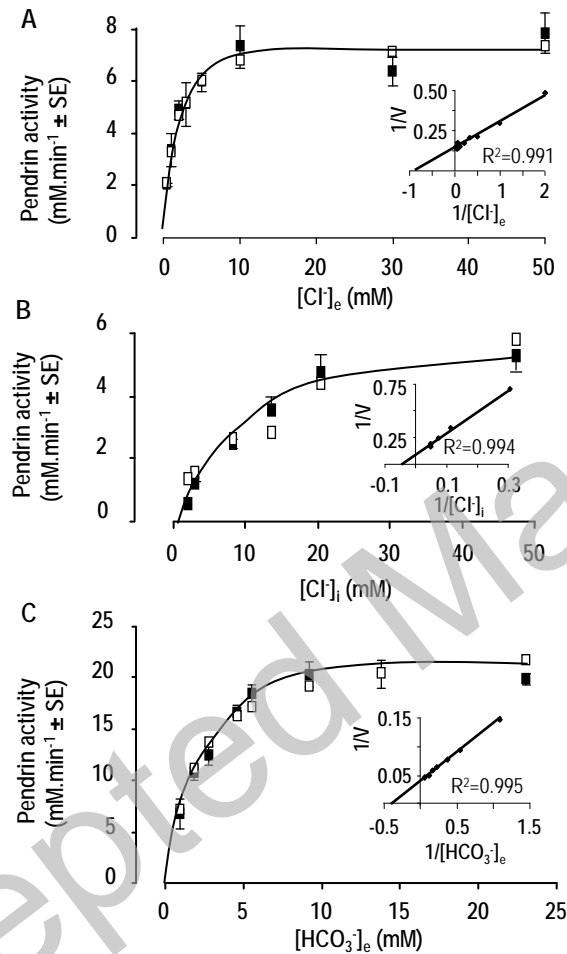


Figure 4. Pendrin activity as a function of anion concentration.

Pendrin activity was measured (black squares) as described in Figure 3 in the presence of different concentrations of Cl⁻, OH⁻ and HCO₃⁻. Also displayed are calculated values (white squares), computed using the mathematical model of pendrin-mediated ion transport. Insets show the Lineweaver-Burk plots of the measured data.

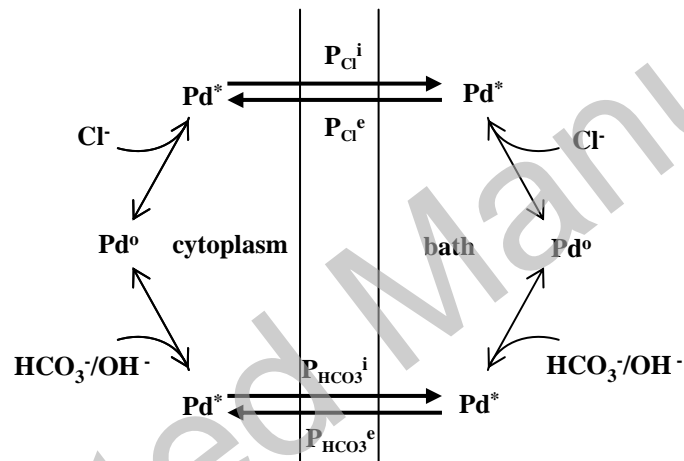


Figure 5. Kinetic scheme of pendrin.

Pendrin-mediated ion transport across the cell membrane is represented according to a ping-pong mechanism. Pd° and Pd* refer to the free and ion-bound forms of pendrin, and P_{Cl} and P_{HCO_3} are the translocation rates of chloride and bicarbonate respectively (see Appendix B for details).

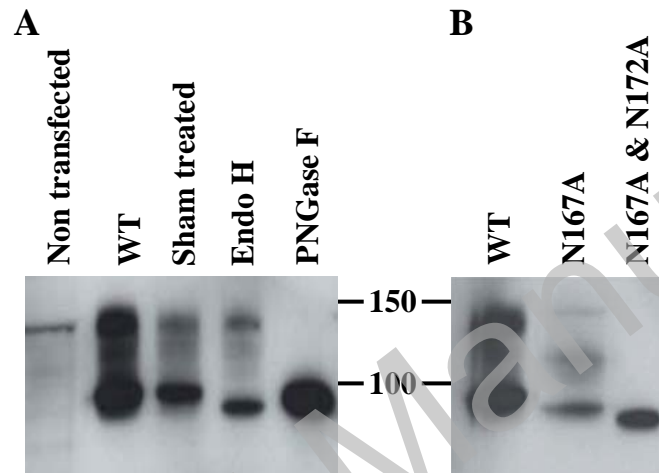


Figure 6. Glycosylation of pendrin.

- A. Electrophoretical profile of pendrin in HEK293 cells transiently transfected with pendrin, in the absence of treatment or after treatment with endoglycosidase H, N glycosidase F, or sham treatment. Note that non-transfected cells display a non specific band at ~ 130 kDa.
- B. Electrophoretical profile of HEK293 cells transiently transfected with wild type pendrin (WT), or mutated pendrin with disruption of either only N167 or both N167 and N172 glycosylation sites.

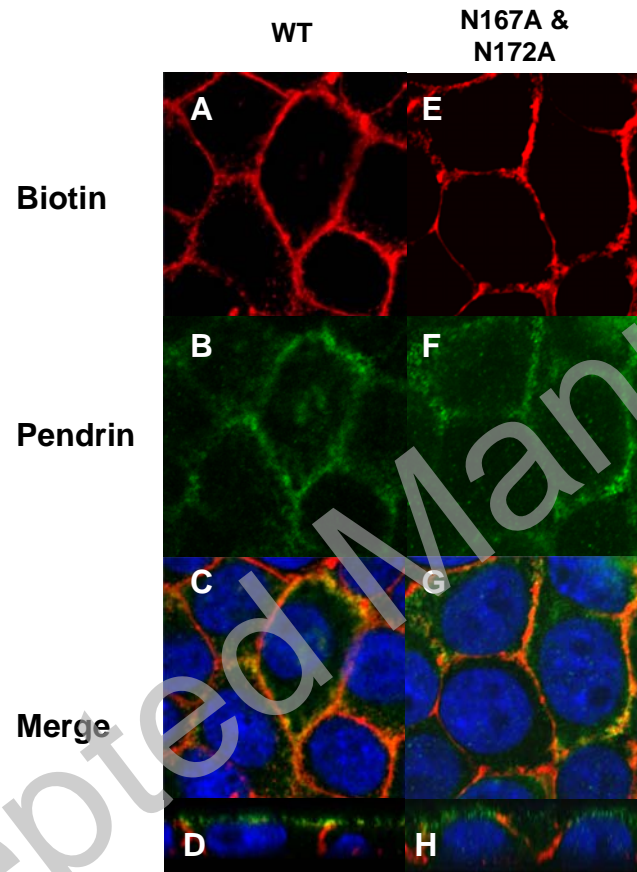


Figure 7. Immunolocalization of pendrin in stably transfected OKP cells.

Confluent OKP cells stably transfected with either wild type (A-D) or N167A/N172A double mutant pendrin (E-H) were biotinylated and then stained for surface biotin (A & E, streptavidin-Cy5) and pendrin (B & F, anti-pendrin antibody followed by FITC-conjugated goat anti-rabbit IgG). The stained slides were visualized by confocal microscopy. C & G show the merges of the two labellings. D & H. show *x-z* reconstructions of confocal microscopy merge image stacks.

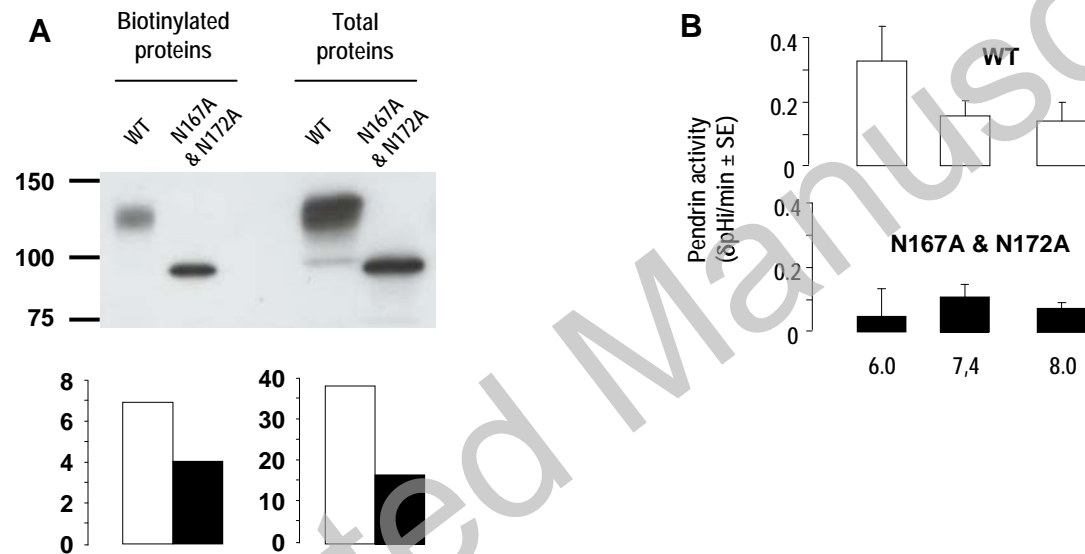


Figure 8. Membrane expression and activity of pendrin with disrupted N-linked glycosylation sites.

- A. Pendrin immunoblot of biotinylated and whole cell proteins in OKP cells stably transfected with either wild type or N167A/N172A double mutant pendrin. The upper panel shows the blot and the lower panel shows the densitometry measurements of all the bands in each lane.
- B. Pendrin activity, measured under forward Cl⁻/OH⁻ exchange mode at different external pH values (6.0, 7.4, and 8.0) in OKP cells stably transfected with either wild type or N167A/N172A double mutant pendrin. Values are means ± SE from 6-9 samples in 2-3 experiments.